Design, synthesis, and biological characterization of a peptide-mimetic antagonist for a tethered-ligand receptor

Patricia Andrade-Gordon*†, Bruce E. Maryanoff*†, Claudia K. Derian*, Han-Cheng Zhang*, Michael F. Addo*, Andrew L. Darrow*, Annette J. Eckardt*, William J. Hoekstra*, David F. McComsey*, Donna Oksenberg‡, Elwood E. Reynolds‡, Rosemary J. Santulli*, Robert M. Scarborough‡, Charles E. Smith*, and Kimberly B. White*

*Drug Discovery, The R. W. Johnson Pharmaceutical Research Institute, Spring House, PA 19477; and ‡COR Therapeutics, Inc., South San Francisco, CA 94080

Edited by Pedro M. Cuatrecasas, University of California, School of Medicine, San Diego, CA, and approved August 13, 1999 (received for review July 6, 1999)

Protease-activated receptors (PARs) represent a unique family of seven-transmembrane G protein-coupled receptors, which are enzymatically cleaved to expose a truncated extracellular N terminus that acts as a tethered activating ligand. PAR-1 is cleaved and activated by the serine protease α-thrombin, is expressed in various tissues (e.g., platelets and vascular cells), and is involved in cellular responses associated with hemostasis, proliferation, and tissue injury. We have discovered a series of potent peptide-mimetic antagonists of PAR-1, exemplified by RWJ-56110. Spatial relationships between important functional groups of the PAR-1 agonist peptide epitope SFLLRN were employed to design and synthesize candidate ligands with appropriate groups attached to a rigid molecular scaffold. Prototype RWJ-53052 was identified and optimized via solid-phase parallel synthesis of chemical libraries. RWJ-56110 emerged as a potent, selective PAR-1 antagonist, devoid of PAR-1 agonist and thrombin inhibitory activity. It binds to PAR-1, interferes with PAR-1 calcium mobilization and cellular function (platelet aggregation; cell proliferation), and has no effect on PAR-2, PAR-3, or PAR-4. By flow cytometry, RWJ-56110 was confirmed as a direct inhibitor of PAR-1 activation and internalization, without affecting N-terminal cleavage. At high concentrations of α-thrombin, RWJ-56110 fully blocked activation responses in human vascular cells, albeit *not* in human platelets; whereas, at high concentrations of SFLLRN-NH_2, RWJ-56110 blocked activation responses in *both* cell types. Thus, thrombin activates human platelets independently of PAR-1, i.e., through PAR-4, which we confirmed by PCR analysis. Selective PAR-1 antagonists, such as RWJ-56110, should serve as useful tools to study PARs and may have therapeutic potential for treating thrombosis and restenosis.

In living organisms, intracellular communication involving cell-surface receptors and native hormones, such as neurotransmitters and growth factors, is crucial to function and survival. G protein-coupled receptors, which are activated by diverse molecules and are targets of a wide selection of drugs (1–6), were thought to be activated by endogenous ligands generated remotely and compelled to travel some distance before interacting with their receptor. However, this picture changed dramatically with the discovery of the first thrombin receptor (protease-activated receptor 1; PAR-1) from human platelet progenitor cells (7). The serine protease α-thrombin cleaves the extracellular, N-terminal peptide chain of PAR-1 between Arg-41 and Ser-42 to expose a truncated N terminus bearing the peptide recognition motif SFLLRN (8). Synthetic peptides containing this epitope have full PAR-1 agonist properties independent of thrombin activation, confirming that the receptor-linked peptide sequence serves as an activating ligand (9). Notably, PAR-1 mediates most of the cellular actions of thrombin, including platelet aggregation, cell proliferation, inflammatory responses, and neurodegeneration (10–13).

Researchers have identified three more members of this class of G protein-coupled receptors, PAR-2 (14–16), PAR-3 (17), and PAR-4 (18, 19), which also are activated by a serine protease to initiate an *intramolecular ligand-activation mechanism*. Given intramolecular binding of a tethered ligand to a cleaved receptor for PAR-1, an external ligand in competition would experience unfavorable energetics because of entropy considerations, thereby making the identification of small molecule antagonists very challenging. Indeed, our initial screening of nearly 200,000 chemical entities from compound libraries for PAR-1 antagonist activity did not yield any worthwhile leads. Thus, we deemed it necessary to design a PAR-1 antagonist *de novo*. After working exploratively with modified agonist peptides to little avail (20–23), we embarked on a peptide-mimetic design concept based on (*i*) structure-function data for PAR-1 agonist peptide epitopes, (*ii*) spatial constraints of groups in the SFLLRN agonist ligand, and (*iii*) a rigid heterocyclic template for spatially displaying key functional groups. This work led to RWJ-53052 (Fig. 1), a prototype PAR-1 antagonist containing an indole template. The structure-function properties of this peptide-mimetic series were optimized via solid-phase parallel synthesis, resulting in improved antagonists, such as RWJ-56110 (Fig. 1). Herein, we report the design, synthesis, and biological characterization of potent peptide-mimetic PAR-1 antagonists, which should serve as useful tools to study PARs and have therapeutic potential for treating thrombosis and restenosis.

Materials and Methods

Synthetic Chemistry. The route used to synthesize prototype antagonist RWJ-53052 (**5**) is depicted in Fig. 2 (experimental details to be reported separately). Products were characterized by ^{1}H NMR (400 or 500 MHz), electrospray fast-atom bombardment MS, and analytical HPLC. The reaction yields are for unoptimized procedures and isolated, purified materials.

Data for RWJ-53052 are ^{1}H NMR (DMSO-d_6) δ 11.12 (s, 1H), 10.28 (m, 1H), 8.85 (s, 1H), 8.50 (t, J = 5.9 Hz, 1H), 8.37 (d, J = 7.9 Hz, 1H), 8.13 (d, J = 9.1 Hz, 2H), 7.7 (m, 4H), 7.0–7.3 (m, 13H), 6.95 (m, 2H), 6.78 (d, J = 8.6 Hz, 2H), 6.32 (d, J = 5.8 Hz, 1H), 5.32 (s, 2H), 4.2–4.5 (m, 6H), 3.69 (s, 3H), 3.10 (m, 4H), 2.97 (m, 1H), 2.75 (m, 1H), 1.3–2.0 (m, 8H); electrospray-MS m/z 790 (MH^+). Analysis ($C_{44}H_{52}FN_9O_4$·2.1 HCl·2.9 H_2O; molecular weight 789.96/918.77): C, H, N, Cl, F within ±0.4%.

Solid-phase parallel synthesis was used to generate diverse analogues of RWJ-53052. The procedures employed (methods A

This paper was submitted directly (Track II) to the PNAS office.

Abbreviations: PAR, protease-activated receptor; Fmoc, 9-fluorenylmethoxycarbonyl; HOBt, 1-hydroxybenzotriazole; DMF, dimethylformamide; HBTU, 2-(1*H*-benzotriazole-1-yl)-1,1,3,3-tetramethyluronium hexafluorophosphate; DCC, 1,3-dicyclohexylcarbodiimide; HMVEC, human microvascular endothelial cells; HASMC, human aortic smooth muscle cells; RASMC, rat aortic smooth muscle cells; RT, reverse transcriptase.

†To whom reprint requests should be addressed. E-mail: pandrade@prius.jnj.com or bmaryano@prius.jnj.com.

The publication costs of this article were defrayed in part by page charge payment. This article must therefore be hereby marked "*advertisement*" in accordance with 18 U.S.C. §1734 solely to indicate this fact.

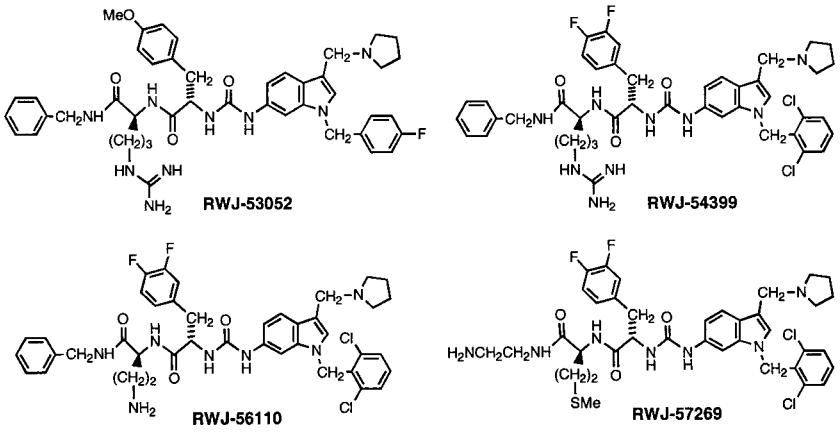

Fig. 1. Structures of peptide-mimetic PAR-1 antagonists.

and B) allowed for alteration of various sites (R^1, R^2, R^3, R^4, and Ar) around the molecule (Fig. 3). The products were characterized normally by MS, analytical HPLC [Supelcosil ABZ+plus column (5 cm × 2.1 mm, 3 μm); 254 or 220 nm detection], and, representatively, by ^{1}H NMR (300, 400, or 500 MHz). Selected compounds were purified by reverse-phase HPLC [three Waters PrepPak cartridges (25 mm × 100 mm; Bondapak C18, 15–20 μm, 125 Å) in series; 254 nm] and characterized by microanalysis.

A typical example is the solid-phase synthesis of RWJ-56110 (**10**), conducted by method A (Fig. 3; details to be reported separately). *N*-α-Fmoc-*N*-γ-Boc-2,4-diaminobutyric acid was coupled with benzylamine (DCC; HOBt), followed by Boc deprotection with trifluoroacetic acid. The resulting amine was loaded onto 2-Cl-trityl-Cl resin and treated with piperidine to afford **7**. Coupling with Fmoc-3,4-difluoro-Phe-OH (HBTU; HOBt) was followed by Fmoc deprotection with piperidine to furnish resin-bound dipeptide **8**. Urea formation between **8** and 6-amino-1-(2,6-dichlorobenzyl)indole was effected with 4-nitrophenylchloroformate to provide **9**. Mannich reaction with pyrrolidine and formaldehyde, followed by resin cleavage with trifluoroacetic acid, afforded crude RWJ-56110 (**10**) with 98% purity (as determined by HPLC). Reverse-phase HPLC provided pure RWJ-56110 (76% overall yield from resin **7**).

Data for RWJ-56110 are ^{1}H NMR (CD_3OD) δ 7.83 (s, 1H), 7.62–7.02 (m, 14H), 5.43 (d, J = 2.7 Hz, 2H), 4.53–4.46 (m, 2H), 4.44 (s, 2H), 4.38 (d, J = 5.6 Hz, 2H), 3.42–3.31 (m, 2H), 3.29–2.93 (m, 6H), 2.22–1.85 (m, 6H); electrospray-MS m/z 790

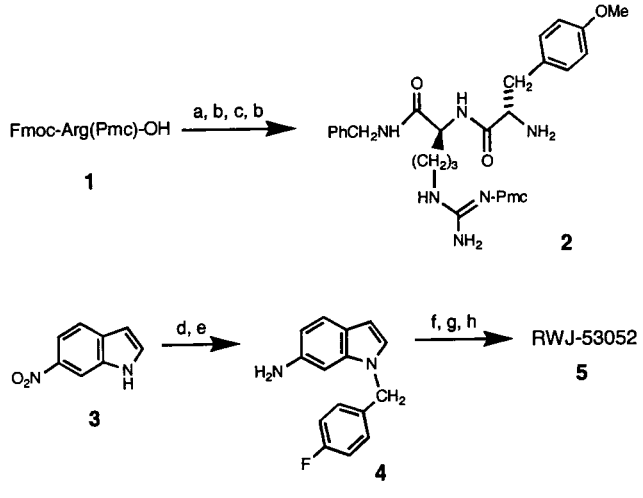

Fig. 2. Synthesis of prototype RWJ-53052 (**5**). Reaction conditions (yield): a, $BnNH_2$, bis(2-oxo-3-oxazolidinyl)phosphinic chloride, CH_2Cl_2, 0°C (83%); b, 20% (vol/vol) piperidine in 1,4-dioxane (99%); c, Fmoc-4-methoxyphenylalanine, 1,3-diisopropylcarbodiimide, HOBt, CH_2Cl_2 (84%); d, 4-fluorobenzyl bromide, Cs_2CO_3, DMF; e, $FeCl_3$·6 H_2O, charcoal powder, Me_2NNH_2, MeOH, reflux (93% for 2 steps); f, 4-nitrophenylchloroformate, *i*-Pr_2NEt, CH_2Cl_2, −20°C—added **2** and warmed to 23°C (65%); g, 37% aqueous CH_2O, pyrrolidine, AcOH (63%); h, CF_3CO_2H/CH_2Cl_2 (97%). Abbreviations: Fmoc, 9-fluorenylmethoxycarbonyl; Pmc, 2,2,5,7,8-pentamethylchroman-6-sulfonyl; HOBt, 1-hydroxybenzotriazole; DMF, dimethylformamide.

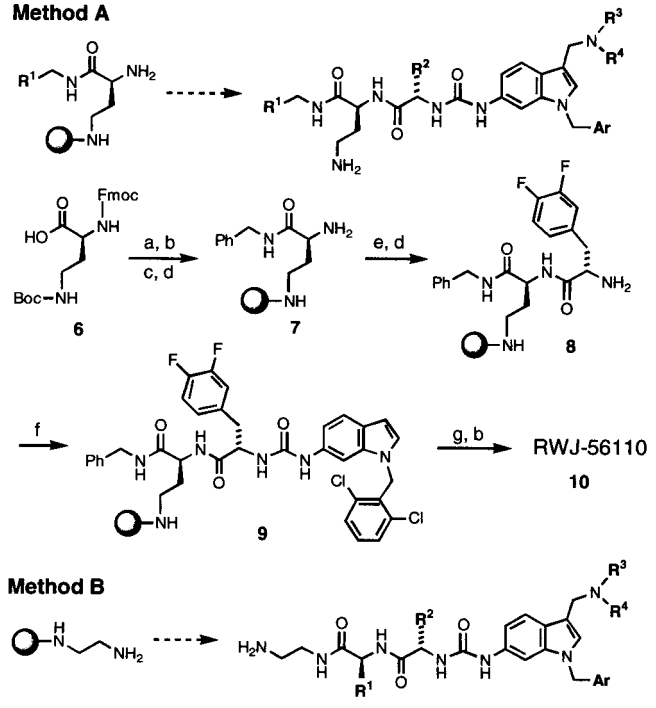

Fig. 3. Solid-phase parallel synthesis of analogues of RWJ-50352 (sphere = 2-chlorotrityl resin). Method A: a, $BnNH_2$, DCC, HOBt, MeCN; b, CF_3CO_2H, CH_2Cl_2; c, 2-Cl-trityl-Cl resin, *i*-Pr_2NEt, CH_2Cl_2-DMF; d, piperidine, DMF; e, Fmoc-3,4-diF-Phe-OH, HBTU, HOBt, *i*-Pr_2NEt, DMF; f, 6-amino-1-(2,6-dichlorobenzyl)indole (prepared as for **4**, Fig. 2), 4-nitrophenylchloroformate, *i*-Pr_2NEt, CH_2Cl_2, −20°C; g, pyrrolidine, 37% aqueous CH_2O, HOAc, 1,4-dioxane. The overall purified yield from resin **7** was 76%. Method B: trityl resin-based synthesis. Abbreviations: DCC, 1,3-dicyclohexylcarbodiimide; HBTU, 2-(1*H*-benzotriazole-1-yl)-1,1,3,3-tetramethyluronium hexafluorophosphate; see Fig. 2.

(MH^+). Analysis ($C_{41}H_{43}Cl_2F_2N_7O_3 \cdot 2.7\ CF_3CO_2H \cdot 0.50\ H_2O$; molecular weight 790.74/1112.18): C, H, N, F within ±0.4%.

Inhibition of Platelet Aggregation. Platelet-rich plasma concentrate (Biological Specialties, Colmar, PA) was gel filtered (Sepharose 2B, Amersham Pharmacia) in Tyrode's buffer (140 mM NaCl/2.7 mM KCl/12 mM $NaHCO_3$/0.76 mM Na_2HPO_4/5.5 mM dextrose/5.0 mM Hepes/2 mg/ml BSA, pH 7.4). Gel-filtered platelets were diluted with Tyrode's buffer (143,000 platelets per μl per well), compound solution in buffer, and 2 mM $CaCl_2$ in a 96-well microtiter plate. Platelet aggregation was initiated by addition of agonist shown to achieve 80% aggregation. The assay plate was mixed gently and constantly. Aggregation was monitored at 0 and 5 min after agonist addition in a microplate reader (Molecular Devices) by optical density at 650 nm (ΔSOFT). Aggregation was calculated as the decrease in optical density between the two measurements.

Cell Cultures. CHRF-288-11 cells were kindly provided by M. Lieberman (University of Cincinnati, Cincinnati; ref. 24). Human microvascular endothelial cells (HMVEC), human aortic smooth muscle cells (HASMC), and their growth media were obtained from Cascade Biologics (Portland, OR). Rat aortic smooth muscle cells (RASMC) were obtained from Cell Applications (San Diego) and were cultured as described (25). Immortalized murine lung myofibroblasts derived from PAR-1-deficient mice (26), which lack functional PAR-1, PAR-2, and PAR-4, were transfected with human PAR-1, PAR-2, or PAR-4 in a modified pCDNA3 construct encoding a hygromycin resistance gene. Stable transfectants were selected in 250 μg/ml hygromycin B and screened by specific agonist-induced calcium mobilization.

PAR-1 Radioligand Binding Assay. CHRF-288-11 cells were washed with PBS, and pellets were homogenized in 20 mM Tris·HCl (pH 7.5) containing 5 mM EDTA and 0.1 mM PMSF; 10 s of sonication followed. Nuclear debris and intact cells were removed by centrifugation at 1,000 × *g* for 10 min. The supernatant was centrifuged at 35,000 × *g* for 30 min, and the pellet was resuspended in 25 mM Tris·HCl, pH 7.5/25 mM $MgCl_2$/10% (vol/vol) sucrose containing 0.1 mM PMSF, 50 μg/ml antipain, 1 μg/ml aprotinin, 40 μg/ml bestatin, 100 μg/ml chymostatin, 0.5 μg/ml leupeptin, and 0.7 μg/ml pepstatin. Protein concentration was determined by the Bradford method. Assays were performed with 25 μg of membrane protein/100 μl and 10 nM [^{3}H]*S*-(*p*-F-Phe)-homoarginine-L-homoarginine-KY-NH_2 (K_d = 15 nM) in the absence or presence of test compound (0.001–100 μM). Nonspecific binding, determined with cold ligand at 25 μM, was ≤20%. Reactions were run in 96-well microtiter plates for 30 min at 23°C and terminated by passage through Whatman GF/C filters (presoaked for 2 h in 10 mM Hepes containing 0.5% polyethyleneimine and 0.1 M *N*-acetylglucosamine), followed by four washes with a Skatron cell harvester (Sterling, VA). Dried filters were assayed in a Wallac MicroBeta counter (Gaithersburg, MD).

Calcium Mobilization. Intracellular calcium mobilization was measured by using a fluorescence technique. Cells in 96-well microtiter plates were loaded with 5 μM fluo-3-AM (Molecular Probes) for 90 min. Plates were washed five times to remove unincorporated dye. Subsequent steps were performed with a Fluorometric Imaging Plate Reader (FLIPR; Molecular Devices). Test compounds were added, and cells were monitored for 5 min to detect any agonist activity. Thrombin or agonist peptide was added, and the fluorescence signal was recorded for 3 min. Net peak calcium, expressed in arbitrary fluorescence units, was measured automatically.

DNA Synthesis. Cell proliferation was measured by [^{14}C]thymidine incorporation. RASMC were plated on Cytostar scintillating plates (Amersham Pharmacia). After 4 days of growth, cells were serum depleted for 4 days (25). Thrombin or agonist peptides were added in fresh medium, and cells were incubated for 24 h. [^{14}C]Thymidine was added, and incubation was continued for 24 h. [^{14}C]Thymidine incorporation was measured in a Wallac MicroBeta counter without additional processing steps.

PCR Analysis for PAR-4. Total RNA from HASMC, gel-filtered platelets, or CHRF-288-11 cells was isolated with TRIzol Reagent (Life Technologies, Grand Island, NY). RNA was converted to cDNA with random primers in the presence of Superscript II reverse transcriptase (RT; Life Technologies) or absence of RT (−RT for negative controls). PCRs were conducted on 50 ng of cDNA or equivalent amounts of RNA in the −RT reactions by using the Advantage-GC cDNA Polymerase Mix (CLONTECH). The sense and antisense primers for the amplification of PAR-4 sequences were hP4#2-U (5′-CTACGACGAGAGCGGGAGCAC-3′) and hP4#2-L (5′-CAGCGCCAGGGCCAGCAGGAGGTC-3′), respectively; for β-actin, they were B-Act.-U (5′-AGGCCAACCGCGAGAAGATG-3′) and B-Act.-L (5′-CTCGGCCGTGGTGGTGAAGC-3′), respectively. Reactions (50 μl) were performed as follows: for PAR-4, 30 cycles of 94°C for 30 s/62.9°C for 30 s/68°C for 45 s; for β-actin, 25 cycles of 94°C for 30 s/60.4°C for 30 s/68°C for 45 s. Each product (5.0 μl) was electrophoresed through 2% agarose gels and transferred to Hybond N+ membranes (Amersham Pharmacia). The appropriate 40-mer primer probes, corresponding to nested sequences in PAR-4 (hP4 PP#2-L: 5′-CCAGCCCATTGGCCGGCAGCCCCACCACCAGGACCAGCCC-3′) and β-actin (B-Act.-PP-L: 5′-TGGGCACAGTGTGGGTGACCCCGTCACCGGAGTCCATCAC--3′), were digoxigenin labeled, hybridized, and detected (Genius nucleic acid system; Roche Molecular Biochemicals).

Flow Cytometry Studies. The activation of PAR-1 on CHRF-288-11 cells was monitored by flow cytometry by using the PAR-1 antibodies SPAN12 and ATAP2, as described (27). Briefly, CHRF-288-11 cells were preincubated with test compound for 5 min and then incubated with thrombin (2 nM) for 10 min at 37°C. Fixed cells were incubated with either ATAP2 or SPAN12 for 30 min at 4°C, followed by secondary conjugation with FITC-labeled goat anti-mouse IgG. Antibody binding was measured with a fluorescence-activated cell sorter (FACScan; Becton Dickinson); antibody bound to unstimulated cells is defined as 100% (control) and represents intact PAR-1.

Results

Design, Synthesis, and Identification of PAR-1 Antagonists. Structure-function studies in terms of platelet activation have been conducted on numerous SFLLRN-based PAR-1 agonist peptides (9, 28–34). Generally speaking, the peptides require at least the N-terminal pentapeptide with a free amino group at position 1, a certain aromatic residue such as phenylalanine at position 2, and a basic residue such as arginine at position 5. With this in mind, we sought to attach amino, phenyl (aryl), and guanidino groups to a rigid molecular scaffold in a suitable pattern, hoping to obtain a worthwhile series of peptide-mimetic PAR-1 antagonists. Our design approach relied on distance parameters taken from models of SFLLRN-NH_2 generated computationally. We obtained low-energy conformations for the agonist hexapeptide by considering extended (β-sheet) and α-helical structures and then applying a molecular dynamics search of energy-minimized conformers to define families of SFLLRN conformers (e.g., see ref. 23). This exercise afforded a "three-point model" with distance ranges between the ammonium group, the center of benzene ring (Phe residue), and the central carbon of the guanidine group (Arg residue; Fig. 4*A*), which were used in conjunction with different rigid molecular templates to design candidate peptide-mimetic

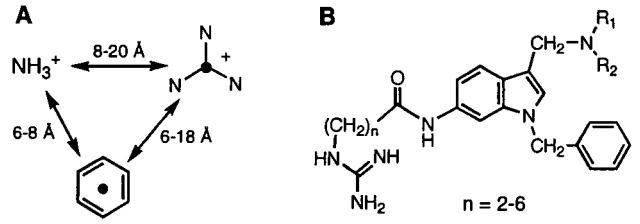

Fig. 4. (*A*) Three-point model showing spatial distribution of the key ammonium, phenyl, and guanidinium groups in the agonist peptide SFLLRN-NH_2 (doubly protonated form). Structural models were assembled computationally in extended and α-helical geometries by using the PROTEIN BUILD command within the BIOPOLYMER mode of the SYBYL software suite (Tripos Associates, St. Louis). The structures were energy minimized (Kollman United Atoms force field; conjugate gradient method) and subjected to molecular dynamics searches (SYBYL; ref. 23). This search provided ranges of distances between the three groups, which were used as a starting point for peptide-mimetic design. (*B*) General formula for template-based SFLLRN-mimetic compounds, based on the distances in *A*.

structures (e.g., Fig. 4*B*). A 6-aminoindole template was among those selected initially, because it met the spatial requirements for displaying the three key substituents and offered favorable synthetic considerations for attachment of the substituents, including readily available starting materials.

We developed a convergent, solution-phase methodology to prepare diverse compounds, including prototype RWJ-53052, which was synthesized in 23% yield from commercial 6-nitroindole. In the synthesis of RWJ-53052 (Fig. 2), two Fmoc-protected amino acids and 6-nitroindole were processed and converted into units **2** and **4**, which were coupled via 4-nitrophenyl chloroformate to give a protected urea precursor of **5** (65% yield). Mannich condensation with pyrrolidine/formaldehyde, followed by trifluoroacetic acid deprotection, afforded desired target **5** (RWJ-53052).

RWJ-53052 inhibited the aggregation of human platelets induced by *both* SFLLRN-NH_2 (IC_{50} = 0.27 μM) and thrombin (IC_{50} = 2.32 μM), while being *quite selective* relative to collagen and the thromboxane mimetic U46619 (Table 1). Also, RWJ-53052 had reasonable affinity for PAR-1 (IC_{50} = 2.2 μM) in a radioligand binding assay (Table 1). Evaluation of RWJ-53052 in nonplatelet functional assays indicated that its potency in inhibiting the effects of thrombin was just moderate. Although it had IC_{50} values in the HMVEC and RASMC calcium mobilization assays of 0.54 and 7.4 μM, respectively, it was weakly active in the RASMC proliferation assay ($IC_{50} > 30$ μM).

To improve this lead, we developed several resin-based, solid-phase syntheses of analogues in which we could alter various sites around the molecule (R^1, R^2, R^3, R^4, and Ar); two of these are depicted in Fig. 3. Numerous derivatives were prepared in parallel as consecutive libraries of 12 compounds each, in an iterative approach toward structure optimization. RWJ-54399, RWJ-56110, and RWJ-57269 were among the more noteworthy derivatives (Fig. 1), as judged by their effects on platelet aggregation induced by SFLLRN-NH_2, thrombin, collagen, and U46619, as well as their affinities for PAR-1 (Table 1). They are potent inhibitors of platelet aggregation induced by *both* SFLLRN-NH_2 and thrombin and are very selective vs. collagen and U46619. Notably, RWJ-57269 had strong affinity for PAR-1 (IC_{50} = 25 nM), although it was cytotoxic at higher concentrations (platelet toxicity: LD_{50} = 37 μM; RASMC toxicity: LD_{50} = 13 μM).

Table 2. RWJ-56110 inhibition of thrombin-induced cellular activity associated with PAR-1 activation

Assay	IC_{50}, μM (no.)*
hPAR-1 Ca^{2+} mobilization†	0.29 ± 0.09 (3)
HMVEC Ca^{2+} mobilization	0.13 ± 0.07 (2)
RASMC Ca^{2+} mobilization	0.12 ± 0.02 (2)
HASMC Ca^{2+} mobilization	0.17 ± 0.06 (2)
RASMC proliferation	3.5 ± 0.5 (4)

*Concentrations of α-thrombin: calcium mobilization, 2.0 nM; cell proliferation, 0.8 nM. Results are expressed as means ± SEM.
†Lung myofibroblasts from PAR-1 deficient mice, transfected with human PAR-1.

Effect of RWJ-56110 on Signaling and Function. On the basis of its potency, selectivity for PAR-1 (see below), and lack of cytotoxicity, we selected RWJ-56110 as a model compound to define PAR-1 antagonism relative to signal transduction and functional activity. RWJ-56110 inhibited thrombin-induced calcium signal transduction in PAR-1-transfected and vascular cells and thrombin-induced proliferation of RASMC (Table 2). Competitive inhibition studies revealed distinct interactions of RWJ-56110 with platelets and vascular cells. At elevated thrombin concentrations, the effectiveness of RWJ-56110 in blocking platelet aggregation and calcium mobilization was reduced in a dose-dependent manner (Fig. 5 *A* and *C*), whereas SFLLRN-mediated responses were inhibited completely (Fig. 5 *B* and *D*). By contrast, full blockade of thrombin's action was observed with RASMC calcium mobilization (Fig. 5*F*) as well as with HMVEC and HASMC calcium mobilization (results not shown). RWJ-56110 also fully inhibited thrombin-induced RASMC proliferation.

The ability of RWJ-56110 to inhibit all signaling and function in RASMC at a full range of thrombin concentrations is significant, because it indicates complete antagonism of the PAR-1 tethered-ligand mechanism. Furthermore, it points to PAR-1 being the only thrombin-sensitive receptor on RASMC, in contrast with platelets where PAR-4 can be operative. Notably, this result reflects the *dual thrombin receptor system*, PAR-1 and PAR-4, in human platelets (18, 19).

Selectivity of RWJ-56110 for PAR-1 vs. Other PARs. To examine PAR-4 in human platelets and vascular cells, CHRF-288-11 cells, HMVEC, and HASMC were evaluated for PAR-4 mRNA expression and functional activity. PCR analysis identified the

Table 1. Inhibition of platelet aggregation and binding to PAR-1

	Platelet aggregation IC_{50}, μM				
RWJ	Thrombin	SFLLRN-NH_2	Collagen	U46619	Binding IC_{50}, μM
53052	2.32 ± 0.11 (184)	0.27 ± 0.01 (172)	IA	IA	2.2 ± 0.5 (23)
54399	0.57 ± 0.21 (8)	0.18 ± 0.21 (10)	IA	IA	0.82 ± 0.34 (4)
56110	0.34 ± 0.04 (13)	0.16 ± 0.06 (15)	IA	IA	0.44 ± 0.21 (6)
57269	0.22 ± 0.08 (4)	0.08 ± 0.03 (3)	4.7 ± 1.5 (2)	24 ± 14 (2)	0.025 ± 0.005 (2)

Concentrations of agonists for aggregation studies: α-thrombin, 0.15 nM; SFLLRN-NH_2, 2 μM; collagen, 3 μg/ml; U46619, 0.3 μM. Results are expressed as means ± SEM with number of experiments (N) in parentheses. IA denotes inactivity at 50 μM of test compound.

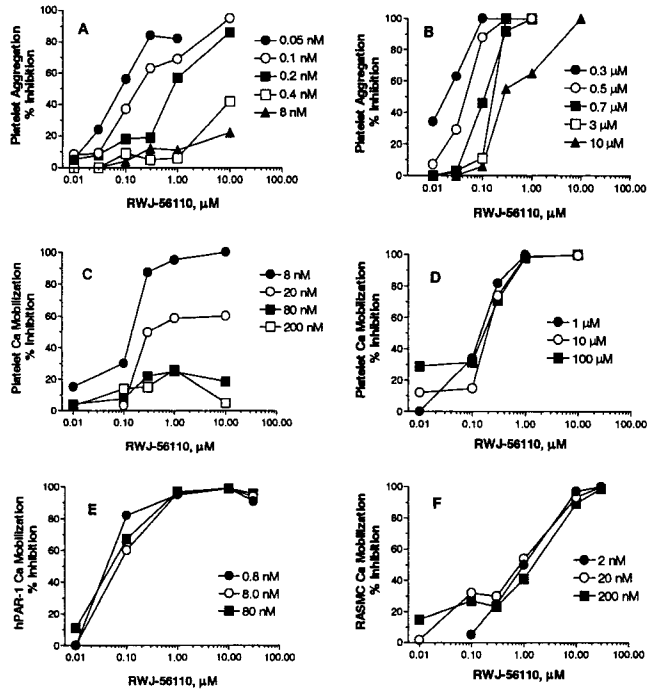

Fig. 5. Inhibitory effects of RWJ-56110 on increasing concentrations of PAR-1 agonists. Platelet aggregation induced by thrombin (*A*) or by SFLLRN-NH_2 (*B*). Platelet calcium mobilization induced by thrombin (*C*) or by SFLLRN-NH_2 (*D*). Calcium mobilization induced by thrombin in lung myofibroblasts from PAR-1-deficient mice, transfected with human PAR-1 (*E*), or in RASMC (*F*).

presence of PAR-4 mRNA in platelets and CHRF-288-11 cells, consistent with previous reports (refs. 18 and 19; Fig. 6); however, there was no PAR-4 mRNA expression in HASMC (Fig. 6). Use of the PAR-4 agonist peptide GYPGKF-NH_2 confirmed that platelets, but not vascular cells, express functionally active PAR-4, with GYPGKF-NH_2 fully activating platelet aggregation (EC_{50} = 61 ± 14 μM). However, GYPGKF-NH_2 did not stimulate calcium mobilization in HMVEC, HASMC, or RASMC (data not shown).

The PAR-1 selectivity of RWJ-56110 was confirmed with transfected cell models wherein murine fibroblasts from PAR-1-deficient mice were transfected with human PAR-1, PAR-2, or PAR-4. RWJ-56110 fully inhibited thrombin-induced calcium responses in cells transfected with PAR-1 (Fig. 5*E*); however, it did not inhibit cells transfected with PAR-2 (trypsin or SLIGRL-NH_2 as the agonist) or PAR-4 (thrombin as the agonist).

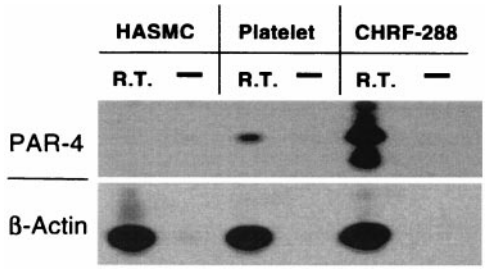

Fig. 6. Expression of PAR-4. Southern blot analysis of PCRs on cDNA samples from RNA of HASMC, gel-filtered platelets, or CHRF-288-11 cells with RT. Control PCRs were done in parallel on each untreated RNA sample (−RT). The primers for the PCRs, the products of which were Southern blotted and probed with the appropriate nested primer probe, corresponded to PAR-4 and the positive control β-actin.

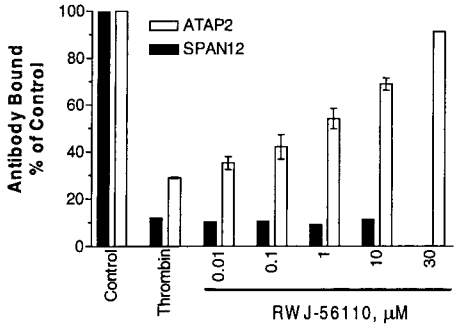

Fig. 7. Inhibition of internalization of cleaved PAR-1 by RWJ-56110. CHRF-288-11 cells were pretreated with increasing concentrations of RWJ-56110 with or without α-thrombin. The surface expression of PAR-1 was monitored by flow cytometry with SPAN12 (solid bars) and ATAP2 (open bars).

Because mouse platelets respond to thrombin by a dual PAR-3/PAR-4 mechanism (19) and because RWJ-56110 does not interact with PAR-4, we studied thrombin-induced aggregation of mouse platelets in the presence of RWJ-56110. Our results (not shown) indicate that RWJ-56110 does not interfere with thrombin-induced mouse platelet aggregation and, hence, does not interact with PAR-3.

Site of Action of RWJ-56110 on PAR-1. Flow cytometry studies with CHRF-288-11 cells were conducted to elucidate RWJ-56110's mechanism of inhibition, capitalizing on antibodies that recognize intact PAR-1 (SPAN12, cleavage sensitive) or PAR-1 in both cleaved and uncleaved states on the cell surface (ATAP2; ref. 27). Stimulation of cells with thrombin causes cleavage and internalization of PAR-1, which is characterized by a loss of SPAN12 *and* ATAP2 binding (Fig. 7). Because RWJ-56110 blocked the loss of ATAP2 binding but not SPAN12 binding, it competes with the tethered ligand to prevent receptor internalization but does not interfere with receptor cleavage. Consistent with these results, RWJ-56110 (100 μM) lacks direct thrombin inhibitory activity.

Discussion

The thrombin receptor PAR-1 mediates many physiological and pathophysiological actions of thrombin at the cellular level. Considering the cellular localization of PAR-1, this receptor probably plays a meaningful role in thrombosis, restenosis, atherosclerosis, proliferative disorders, inflammation, and neurodegeneration. Therefore, the development of potent, small-molecule PAR-1 antagonists would be worthwhile to establish the potential therapeutic utility of blocking thrombin's action on cells, as opposed to blocking thrombin's actions on hemostatic proteins. Among the few examples of PAR-1 antagonists reported (20, 21, 34–38), the molecules of interest are deficient as drug candidates because of two or more of the following attributes: weak potency; peptide constitution; failure to block the action of thrombin on platelets in a consistent manner, although reasonably blocking the action of agonist peptides; mixed agonist/antagonist activity; and lack of good receptor/functional selectivity. The report of Bernatowicz *et al.* (35) stands out by providing peptide compounds with potent antagonist activity in platelet aggregation induced by a PAR-1 agonist peptide (SFLLRNP-NH_2) and with high PAR-1 affinity. For instance, BMS-197525, an archetypal antagonist in this work (35), blocked SFLLRNP-NH_2-induced platelet aggregation with an IC_{50} of 0.20 μM, while being selective relative to ADP and U46619, and bound to PAR-1 with an IC_{50} of 0.008 μM. However, in contrast with its ability to block platelet aggregation and signal transduction events induced by SFLLRNP-NH_2,

BMS-197525 was considerably less potent, and less consistent in interfering with the action of thrombin (35).

Our design approach has led to a heterocyclic template-based peptide-mimetic series of potent antagonists of PAR-1, overcoming the challenge of competing with a tethered-ligand for its receptor. RWJ-56110 blocks platelet aggregation induced by *both* SFLLRN-NH_2 and thrombin with good and *nearly equivalent* potency. This PAR-1 antagonist is functionally selective relative to collagen and U46619 and is selective for PAR-1 relative to PAR-2, PAR-3, and PAR-4. Also, RWJ-56110 inhibits binding of the tethered ligand to PAR-1 after thrombin cleavage, regardless of the thrombin concentration, as evidenced by results in the cells transfected with PAR-1.

The results presented herein indicate that signaling through both PAR-1 and PAR-4 is involved in human platelet activation by thrombin. The evidence principally derives from the observation that RWJ-56110 is completely effective in inhibiting human platelet aggregation induced by any concentration of SFLLRN-NH_2, whereas *it shows diminished antagonism of thrombin at high enzyme concentrations*. This observation supports the presence of another functional PAR, probably PAR-4, which is activated by thrombin at high concentrations (18, 19), in agreement with the recently reported synergism of PAR-1 and PAR-4 blockade in high-dose, thrombin-dependent platelet activation (39). With this information, it becomes unclear whether PAR-1, PAR-4, or both are crucial in thrombotic disease in humans. For instance, the elevated thrombin concentration at the site of vascular injury may induce platelet activation, not only via PAR-1, but also via PAR-4. Thus, the possibility exists that antagonism of PAR-1 will be insufficient to gain a positive therapeutic outcome for the treatment of thrombosis. On the other hand, compromising platelet function only at lower concentrations of thrombin may prove attractive to overcome the bleeding liability associated with powerful antiplatelet agents, such as fibrinogen receptor (GPIIb/IIIa) antagonists. These questions are critical to the design of antithrombotic agents with different mechanisms of action, such as selective PAR-1 antagonists. The availability of antagonists such as RWJ-56110 should assist in resolving these issues.

The cellular actions of thrombin also have been implicated in proliferative events associated with restenosis, tissue remodeling/permeability, and the maintenance of vascular tone (10–13). We found that PAR-4 is not present in vascular cells and that RWJ-56110 is completely effective in blocking thrombin signaling in these cells, independent of thrombin concentration. The mediation of the vascular actions of thrombin via PAR-1 is relevant to proliferative diseases of the vascular wall where thrombin can trigger replication of smooth muscle cells. In this scenario, a PAR-1 antagonist such as RWJ-56110 might be a useful therapeutic agent for the management of restenosis or atherosclerosis.

In summary, RWJ-56110 exemplifies a selective PAR-1 antagonist that competes effectively against the challenging energetics of the tethered-ligand mechanism of a protease-activated G protein-coupled receptor. As such, it represents a key step in the development of a class of therapeutic agents for vascular medicine. Significantly, RWJ-56110 should provide a valuable tool to help elucidate the role of various thrombin receptors in human physiology and disease.

We thank Drs. Harold Almond and Mary-Pat Beavers for computational studies, Mr. John Longo for excellent technical assistance, and Prof. Lawrence Brass (University of Pennsylvania, Philadelphia) for providing the antibodies SPAN12 and ATAP2 and many helpful discussions.

1. Jackson, T. (1991) *Pharmacol. Ther.* **50,** 425–442.
2. Trumpp-Kallmeyer, S., Hoflack, J., Bruinvels, A. & Hibert, M. (1992) *J. Med. Chem.* **35,** 3448–3462.
3. Strader, C. D., Fong, T. M., Tota, M. R., Underwood, D. & Dixon, R. A. F. (1994) *Annu. Rev. Biochem.* **63,** 101–132.
4. Strader, C. D., Fong, T. M., Graziano, M. P. & Tota, M. R. (1995) *FASEB J.* **9,** 745–754.
5. Gudermann, T., Nürnberg, B. & Schultz, G. (1995) *J. Mol. Med.* **73,** 51–63.
6. Moereels, H., Lewi, P. J., Koymans, L. M. H. & Janssen, P. A. J. (1996) *Recept. Channels* **4,** 19–30.
7. Vu, T.-K. H., Wheaton, V. I., Hung, D. T. & Coughlin, S. R. (1991) *Cell* **64,** 1057–1068.
8. Coughlin, S. R. (1993) *Thromb. Haemostasis* **70,** 184–187.
9. Scarborough, R. M., Naughton, M., Teng, W., Hung, D. T., Rose, J., Vu, T.-K. H., Wheaton, V. I., Turck, C. W. & Coughlin, S. R. (1992) *J. Biol. Chem.* **267,** 13146–13149.
10. Ogletree, M. L., Natarajan, S. & Seiler, S. M. (1993) *Perspect. Drug Discovery Des.* **1,** 527–536.
11. Coughlin, S. R. (1994) *Trends Cardiovasc. Med.* **4,** 77–83.
12. Dennington, P. M. & Berndt, M. C. (1994) *Clin. Exp. Pharmacol. Physiol.* **21,** 349–358.
13. Van Obberghen-Schilling, E., Chambard, J.-C., Vouret-Craviari, V., Chen, Y.-H., Grall, D. & Pouysségur, J. (1995) *Eur. J. Med. Chem.* **30,** Suppl., 117–130.
14. Nystedt, S., Emilsson, K., Wahlestedt, C. & Sundelin, J. (1994) *Proc. Natl. Acad. Sci. USA* **91,** 9208–9212.
15. Nystedt, S., Emilsson, K., Larsson, A.-K., Stroembeck, B. & Sundelin, J. (1995) *Eur. J. Biochem.* **232,** 84–89.
16. Nystedt, S., Larsson, A. K., Aberg, H. & Sundelin, J. (1995) *J. Biol. Chem.* **270,** 5950–5955.
17. Ishihara, H., Connolly, A. J., Zeng, D., Kahn, M. L., Zheng, Y.-W., Timmons, C., Tram, T. & Coughlin, S. R. (1997) *Nature* (*London*) **386,** 502–506.
18. Xu, W.-F., Andersen, H., Whitmore, T. E., Presnell, S. R., Yee, D. P., Ching, A., Gilbert, T., Davie, E. W. & Foster, D. C. (1998) *Proc. Natl. Acad. Sci. USA* **95,** 6642–6646.
19. Kahn, M. L., Zheng, Y.-W., Huang, W., Bigornia, V., Zeng, D., Moff, S., Farese, R. V., Jr., Tam, C. & Coughlin, S. R. (1998) *Nature* (*London*) **394,** 690–694.
20. Hoekstra, W. J., Hulshizer, B. L., McComsey, D. F., Andrade-Gordon, P., Kauffman, J. A., Addo, M. F., Oksenberg, D., Scarborough, R. M. & Maryanoff, B. E. (1998) *Bioorg. Med. Chem. Lett.* **8,** 1649–1654.
21. McComsey, D. F., Hecker, L. R., Andrade-Gordon, P., Addo, M. F. & Maryanoff, B. E. (1999) *Bioorg. Med. Chem. Lett.* **9,** 255–260.
22. McComsey, D. F., Hawkins, M. J., Andrade-Gordon, P., Addo, M. F., Oksenberg, D. & Maryanoff, B. E. (1999) *Bioorg. Med. Chem. Lett.* **9,** 1423–1428.
23. Ceruso, M. A., McComsey, D. F., Leo, G., Andrade-Gordon, P., Addo, M. F., Scarborough, R. M. Oksenberg, D. & Maryanoff, B. E. (1999) *Bioorg. Med. Chem.* **7,** in press.
24. Jones, C. L. A., Witte, D. P., Feller, M. J., Fugman, D. A., Dorn, G. W., II, & Lieberman, M. A. (1992) *Biochim. Biophys. Acta* **1136,** 272–282.
25. Owens, G. K., Loeb, A., Gordon, D. & Thompson, M. M. (1986) *J. Cell Biol.* **102,** 343–352.
26. Darrow, A. L., Fung-Leung, W.-P., Ye, R. D., Santulli, R. J., Cheung, W.-M., Derian, C. K., Burns, C. L., Damiano, B. P., Zhou, L., Keenan, C. M., *et al.* (1996) *Thromb. Haemostasis* **76,** 860–866.
27. Brass, L. F., Pizarro, S., Ahuja, M., Belmonte, E., Blanchard, N., Stadel, J. M. & Hoxie, J. A. (1994) *J. Biol. Chem.* **269,** 2943–2953.
28. Hui, K. Y., Jakubowski, J. A., Wyss, V. L. & Angleton, E. L. (1992) *Biochem. Biophys. Res. Commun.* **184,** 790–796.
29. Sabo, T., Gurwitz, D., Motola, L., Brodt, P., Barak, R. & Elhanaty, E. (1992) *Biochem. Biophys. Res. Commun.* **188**, 604–610.
30. Chao, B. H., Kalkunte, S., Maraganore, J. M. & Stone, S. R. (1992) *Biochemistry* **31,** 6175–6178.
31. Vassallo, R. R., Jr., Kieber-Emmons, T., Cichowski, K. & Brass, L. F. (1992) *J. Biol. Chem.* **267,** 6081–6085.
32. Feng, D. M., Veber, D. F., Connolly, T. F., Condra, C., Tang, M.-J. & Nutt, R. F. (1995) *J. Med. Chem.* **38,** 4125–4130.
33. Natarajan, S., Reixinger, D., Peluso, M. & Seiler, S. M. (1995) *Int. J. Pept. Protein Res.* **45,** 145–151.
34. Seiler, S. M., Peluso, M., Tuttle, J. G., Pryor, K., Klimas, C., Matsueda, G. R. & Bernatowicz, M. S. (1996) *Mol. Pharmacol.* **49,** 190–197.
35. Bernatowicz, M. S., Klimas, C. E., Hartl, K. S., Peluso, M., Allegretto, N. J. & Seiler, S. M. (1996) *J. Med. Chem.* **39,** 4879–4887.
36. Lindahl, A. H., Scarborough, R. M., Naughton, M. A., Harker, L. A. & Hanson, S. R. (1993) *Thromb. Haemostasis* **69,** 1196.
37. Fujita, T., Nose, T., Nakajima, M., Inoue, Y., Shimohigashi, Y. & Ohno, M. (1997) *Peptide Chemistry*, ed. Kitada, C. (Protein Res. Foundation, Osaka), pp. 233–236.
38. Seiler, S. M., Peluso, M., Michel, I. M., Goldenberg, H., Fenton, J. W., II, Riexinger, D. & Natarjan, S. (1995) *Biochem. Pharmacol.* **49,** 519–528.
39. Kahn, M. L., Nakanishi-Matsui, M., Shapiro, M. J., Ishihara, H. & Coughlin, S. R. (1999) *J. Clin. Invest.* **103,** 879–887.